Journal of King Saud University – Science 33 (2021) 101527

Contents lists available at ScienceDirect

Journal of King Saud University – Science

journal homepage: www.sciencedirect.com

Original article

Biogenic AgNPs for the non-cross-linking detection of aluminum in aqueous systems

Priyanka Joshi [a], Meena Nemiwal [b], Abdullah A. Al-Kahtani [c], Mohd Ubaidullah [c,*], Dinesh Kumar [d,*]

[a] Department of Chemistry, Banasthali Vidyapith, Rajasthan 304022, India
[b] Department of Chemistry, Malaviya National Institute of Technology, Jaipur 302017, India
[c] Department of Chemistry, College of Science, King Saud University, Riyadh 11451, Saudi Arabia
[d] School of Chemical Sciences, Central University of Gujarat, Gandhinagar 382030, India

ARTICLE INFO

Article history:
Received 8 March 2021
Revised 20 May 2021
Accepted 16 June 2021
Available online 24 June 2021

Keywords:
Non-cross-linking detection
Biomediated AgNPs
Cinchona bark extract
Al^{3+} ions

ABSTRACT

Nanoparticle synthesis is one of the most innovative areas of the 21st century in which the implication of the experimental biogenesis process is significant. We report biogenesis of silver nanoparticles (AgNPs) using cinchona bark extract in which cinchona bark extract acts as a reducing agent and stabilizing agent and does not require additional reducing and stabilizing agent. The cinchona-silver nanoparticles (C-AgNPs) were monodispersed with a size of 3–4 nm, stable, highly selective, and used for non-cross-linking detection of aqueous Al^{3+} ion colorimetrically. C-AgNPs provide a good limit of detection (LOD) of 0.01 ppm for Al^{3+} that is well below the detection limit set by USEPA (50 ppm) and WHO (0.199 ppm) and is based on the deep yellow to brown color tuning of the C-AgNPs based detection system. The synthesis of C-AgNPs was optimized in terms of pH, concentration of extract, and the effect of temperature. Morphology and the size of AgNPs were characterized by HRTEM and DLS analysis. Thus, without an additional noxious agent and any labeling agent that is required for cross-linking, a simple, fast, and selective colorimetric method is proposed for ultrasensitive detection of health hazardous aluminum ions. Moreover, this non-toxic, biocompatible plant extract allows the successful detection of Al^{3+} ions in real water samples.

1. Introduction

Nanoscience is one of the most recent developing field and finds applications in various modern technologies such as hydrogen storage, photocatalysis, green energy devices (Nozik, 2010), sensors, biomedical implants (Bhuvaneswari et al., 2021; Serrano et al., 2009), and photovoltaics (Colmenares et al., 2009). Although the most common method used to prepare nanostructures is chemical synthesis (Al-Hartomy et al., 2013; Dhillon et al., 2017a, 2017b), that needs expensive instruments, and chemicals. Therefore, economically viable, and bio-compatible nanoparticles steer toward green chemistry. Surface modification in the synthesis of NPs is significant for controlling the size of NPs, either by increasing colloidal stability or by adding functionality to the NPs. Colloidal stability is maintained by steric and electrostatic forces required for maintaining repulsive force necessary for preventing aggregation of NPs in aqueous solution(Olenin, 2019; Vergara-Barberán et al., 2017). However, these cross-linking colorimetric detections have been employed by many researchers for the application of identification, specific labeling agents (aptamer, peptides, and oligonucleotides) due to the need for a time-consuming and tedious process. Thus, these may be replaced by non–cross-linking detection, which has been investigated for the detection of DNA targets (Dhillon et al., 2018). With this, we use the non-cross-linking approach, which is being applied with rapid and selective detection of metal ions. Biomed synthesis of nanostructures satisfies the entire requirements, especially waste, reducing the use of reducing chemical hazards, thus preventing pollution (Al-Enizi et al., 2020). Moreover, the dual role of biomass as a reducing and stabilizing agent minimizes the complexity of the synthesis procedure[11]. Many of the heavy metal ions are toxic even in trace amounts; their sensing and quantification are urgent

* Corresponding authors.
E-mail addresses: mtayyab@ksu.edu.sa (M. Ubaidullah), dinesh.kumar@cug.ac.in (D. Kumar).
Peer review under responsibility of King Saud University.

Production and hosting by Elsevier

https://doi.org/10.1016/j.jksus.2021.101527
1018-3647/

issues to be addressed. Much attention has been focused on aluminum (Al^{3+}) sensing as it is not a biologically essential element. An increased amount of Al^{3+} in the human body causes damage to the nervous system, loss of memory, listlessness, and Alzheimer's disease (Shaw and Tomljenovic, 2013). Al^{3+} is also responsible for intoxication in hemodialysis patients (Sorenson et al., 1974). This increased amount is toxic for growing plants and water animals (Sorenson et al., 1974).

Therefore, a highly selective, sensitive, and on-site detection of Al^{3+} is needed to avoid its hazardous effects. Several techniques have been used to detect low levels of Al^{3+} ions in various samples. For instance, atomic absorption spectrometry (AAS), fluorimetry, inductively coupled plasma mass spectroscopy (ICP-MS), inductively coupled plasma emission spectrometry (ICP-AES), fluorescent, and liquid chromatography-mass spectrometry (LC-MS) etc. However, background signals, the requirement of professional operators, longer assay time, and complicated synthesis procedures limit their application. Nanoparticles show an extensive application in the detection of heavy metal ions (Firdaus et al., 2017; Li et al., 2010). Although very limited sensors have been reported for the colorimetric detection of the Al^{3+} ion, most of them were synthesized using chemical methods (Chen et al., 2013; Xue et al., 2014). Ascorbic acid capped gold nanoparticles (AA-AuNPs) were used for facile and simple colorimetric detection of Al^{3+} in aqueous media (Kim et al., 2018). Au NPs have been used for aluminum detection by functionalization with a capping of 4-Benzoyl pyrazolone (Rastogi et al., 2017), casein peptide (Abubaker et al., 2018), 5-Hydroxy indole-2-carboxylic acid (5H-I2CA) (Shinde et al., 2017) etc. Although silver nanoparticles show excellent detection properties and have been used to detect many metal ions such as Fe^{2+} (Basiri et al., 2018), Pb^{2+} (Naushad, 2014), Cd^{2+} Cu^{2+}, Co^{2+}, Pb^{2+} and Ni^{2+} (Modrzejewska-Sikorska and Konował, 2020; Zafer et al., 2020), Cr^{3+}(Gao et al., 2020), Hg^{2+} (Faghiri and Ghorbani, 2019) but very little explored for Al^{3+} detection. On the other hand, the-state-of-the-art biogenic nanoparticles fulfill the ultimate needs of sensing the metal ions in the biological system. We report a facile and biocompatible method for synthesizing very small AgNPs with high monodispersity and exploring their use as a highly selective and sensitive sensor for Al^{3+}. Silver nanoparticles were synthesized by green biomasses such as Ficus benjamina leaves (Puente et al., 2019), Carica papaya (Achan et al., 2011).

We used cinchona bark extract as a multifunctional agent to synthesize and stabilize AgNPs and detect Al^{3+} ions. The cinchona bark has long been used in the treatment of malaria and various other medicinal activities (Vinod Kumar et al., 2014). Our proposed method is easy to use because it does not require sophisticated laboratory conditions, applies to room temperature, and works near physical pH. The use of water as a medium in this method enhances its usefulness in various water samples.

2. Materials and methods

Silver nitrate ($AgNO_3$) from (Merck India) and metal salts calcium chloride ($CaCl_2$), ferrous chloride ($FeCl_2$), ferric chloride ($FeCl_3$), barium chloride ($BaCl_2$), zinc chloride ($ZnCl_2$), cadmium chloride ($CdCl_2$), mercuric chloride ($HgCl_2$), lead chloride ($PbCl_2$), copper sulphate pentahydrate ($CuSO_4{\cdot}5H_2O$), manganese chloride ($MnCl_2$), chromium trichloride ($CrCl_3$), aluminum chloride ($AlCl_3$), and NaOH procured from Sigma-Aldrich, and Merck, India were used as received to test the selective colorimetric sensitivity of the AgNPs probe to the metal ions Ca^{2+}, Fe^{2+}, Fe^{3+}, Ba^{2+}, Zn^{2+}, Cd^{2+}, Hg^{2+}, Pb^{2+}, Cu^{2+}, Mn^{2+}, Cr^{3+}, and Al^{3+}. Stock and other aqueous solutions were prepared to rule out any possible analytical measurement interference using Millipore water. All the glassware was thoroughly washed with freshly prepared aqua regia and thoroughly washed with Millipore water before use. The characterization part described in supplementary as Text S-1, preparation of cinchona extract elaborated as Text S-2 and preparation of C-AgNPs as Text S-3.

2.1. Colorimetric selectivity test of C-AgNPs

The selectivity step was crucial in cutting down finally to one specific heavy metal ion to which the developed C-AgNPs probe was colorimetrically sensitive. Aqueous solutions of all metal ions were prepared by dissolving their respective salts in Millipore water and stored at room temperature. To scrutinize the recognition ability of C-AgNPs probe towards metal ions, 200 μL of the previously prepared metal ion solutions were added to the 500 μL of C-AgNPs. The test solutions were allowed to stand for 25 min at room temperature. UV–Vis spectra checked the changes in the color of the test solution. This helped to achieve precise and interference-free detection of Al^{3+} ions.

2.2. Quantitative analysis of Al^{3+} using C-AgNPs

To quantitatively deduce the LOD of C-AgNPs for Al^{3+}, various concentrations of Al^{3+} were prepared by serial dilution of stock solution. From the prepared Al^{3+} solutions, 200 μL each was added separately into 500 μL of AgNPs solution. The solutions were checked for the color change, and after completion of the reaction, the UV–Vis spectra of the solution were recorded.

2.3. Application of the sensor

To confirm the practical applicability of synthesized detection probe (C-AgNPs), pond water and drinking water samples were collected from our campus and research laboratory (Banasthali University, Jaipur, India) and used as such without filtration. The collected samples were spiked with different concentrations of Al^{3+} (0.2 ppm and 0.6 ppm) and analyzed by the procedure mentioned above.

3. Results and discussion

3.1. Formation of C-AgNPs

3.1.1. UV–Vis spectra and HRTEM images

The formation of AgNPs was confirmed by a change in color of the solution from colorless to yellow as a straightforward approach upon the addition of extract to it at room temperature. The UV–Vis spectra of pure plant extract peaked at 279 nm (Fig. 1a) due to the π-π^* transition. This peak disappeared in the UV–Vis spectra of synthesized AgNPs at room temperature. A new sharp characteristic peak was seen at 402 nm due to the excitation of gaseous electrons from the highest occupied cluster orbital to the lowest unoccupied orbital (Fig. 1b). The disappearance of the peak at 279 nm confirms the participation of easily excitable electrons in reducing Ag^+ to Ag^0. C-AgNPs synthesized at 80 ℃ showed a red-shift in peak position to 417 nm with a decrease in intensity (Fig. 1c). A comparison of full-width half maximum (fwhm) values was obtained for the particles synthesized at room temperature (Fig. S 1a) and by heating method (Fig. S 1b). A smaller value of fwhm suggests the synthesis of monodispersed particles, while a higher value results due to particles' polydispersity. Thus, a higher value of fwhm (111 nm) for the particles synthesized by heating supports poly-dispersed particles' synthesis.

In comparison, the lower value of fwhm (97 nm) for the particles synthesized at room temperature supports monodispersed

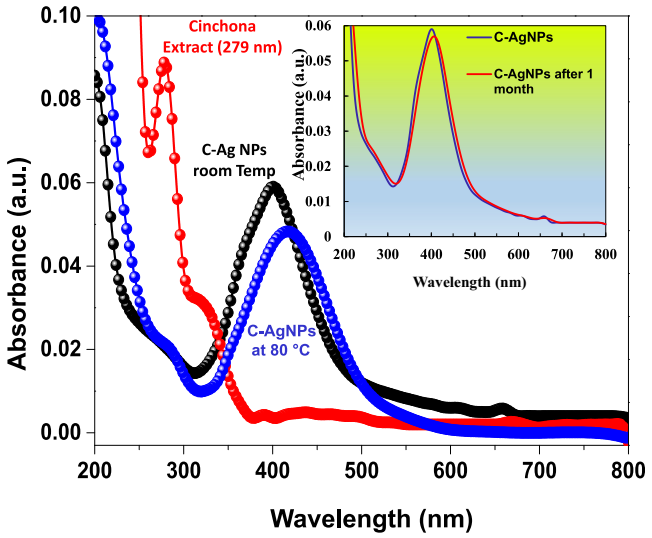

Fig. 1. UV–Vis spectra of cinchona bark extract (a), C-AgNPs at room temperature (b), and at 80 °C (c).

nanoparticles' synthesis. These results were further confirmed by the corresponding HRTEM images of C-AgNPs (Fig. 2a and b). Moreover, the results show that the particles synthesized at room temperature could be more useful for sensitive detection of metal ions. The prepared AgNPs were stable up to a month at room temperature, and their stability was confirmed by SPR spectra (Fig. S2).

3.1.2. FT-IR spectra

The active constituents in most plant extracts are polyphenols, flavonoids, and alkaloids (Kacprzak, 2013). These active constituents are well known for their antioxidant activity, which is an indirect measure of their reducing power (2010). Consequently, these active components can reduce and stabilize the nanoparticles.

We utilized cinchona bark extract for the synthesis of nanoparticles. Cinchona alkaloids are the major components of bark extract (Kacprzak, 2013). The main alkaloids present in the extract are quinine, cinchonidine, quinidine, and cinchonine. Many of their close derivatives that share their basic skeleton with the difference in their side chains have been found in the bark (Kacprzak, 2013). Therefore, it is probable that these alkaloids impart reducing characteristics to the bark extract, which is exploited in the present work for the synthesis of C-AgNPs by the reduction of Ag^{+} to Ag^{0}. We performed FT-IR measurement of the cinchona bark extract and C-AgNPs to confirm alkaloids' presence and their involvement in the reduction (Dictionary of Alkaloids, 2010).

The FT-IR spectra of the extract before the reduction of Ag^{+} show characteristic peaks at 3414 cm^{-1}, 2924 cm^{-1}, 1616 cm^{-1}, 1318 cm^{-1}, 1279 cm^{-1}, and 1060 cm^{-1}, which may be associated with –OH, C – H, CH = CH_2, aromatic and aliphatic C—N, respectively (Fig. 3a). The data show the presence of alkaloids as the major components in the extract. After the reduction of Ag^{+} to Ag^{0}, peaks at 3414 cm^{-1}, 1616 cm^{-1}, 1279 cm^{-1}, and 1060 cm^{-1} disappeared while slight shift was observed in peaks at 1313 $cm^{-1}$to 1360 cm^{-1} (Fig. 3b). These changes in FT-IR spectra show the involvement of alkaloids in the reduction process.

Accordingly, we propose a possible mechanism of reduced synthesis of C-AgNPs (Scheme 1). In the basic medium –OH group tends to lose its hydrogen as a proton, which was confirmed by a decline in the medium's pH as the reaction proceeds. In addition, the high basicity of aliphatic N also supports the reduction process. Likewise, the disappearance of the peak at 1616 cm^{-1} in the C-AgNPs spectrum supports the vinyl group's involvement in the reduction process. After the reduction due to the high affinity of Ag to N, it attaches to the surface of nanoparticles in such a way that the negatively charged oxygen protrudes out in the solution to provide electrostatic stability to the C-AgNPs.

3.2. Role of pH and cinchona bark extract concentration on the synthesis of C-AgNPs

We have observed in our previous studies (Joshi et al., 2017) that bioprocess parameters such as pH and plant extract concentration play a vital role in the synthesis of nanoparticles. Here, we studied the effect of pH and cinchona bark extract concentration on nanoparticles' synthesis at room temperature.

3.2.1. Effect of volume of extract

To study the effect of volume of cinchona bark extract, the reaction was conducted in the presence of various volumes ranging from 50 µL to 2000 µL, and the formation of AgNPs was monitored by UV–Vis spectrophotometer (Fig. 4). The results showed that at minimum volume (50 µL), no peak was observed in the visible region and on increasing the volume of extract from 250 µL to 1000 µL, a continuous increase in the intensity of peak was observed along with a shift in peaks from 419 nm to 402 nm (blue shift). After that, only a slight change in peak intensity was observed on increasing volume from 1000 µL to 2000 µL, indicating completion of the reaction. Accordingly, the colorless solution of $AgNO_3$ gradually changed to yellow with the volume of plant extract, as shown in inset of Fig. 4. Therefore, 1000 µL was selected as an optimized volume to synthesize C-AgNPs.

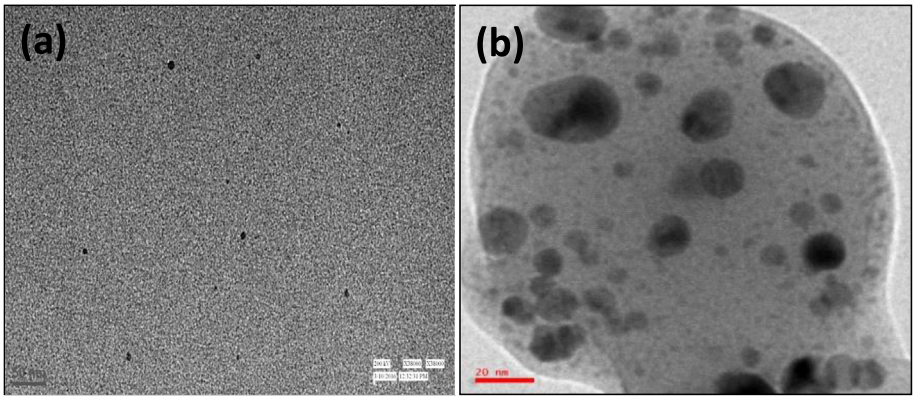

Fig. 2. TEM images of C-AgNPs synthesized at room temperature (a) and at 80 °C (b).

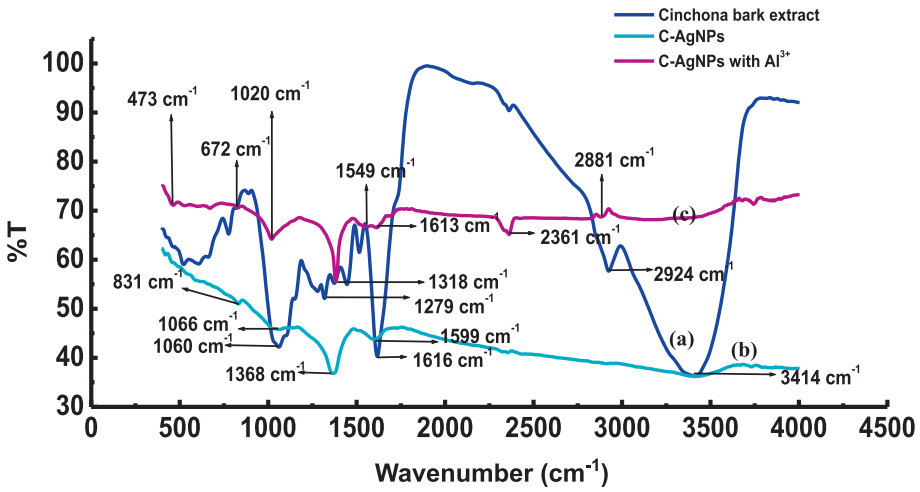

Fig. 3. FT-IR spectra of cinchona extract (a), C-AgNPs (b), and C-AgNPs in the presence of Al^{3+} (c).

Scheme 1. Schematic representation of the synthesis of C-AgNPs and their aggregation in the presence of Al^{3+}.

3.2.2. Effect of pH

The reaction mixture's pH was adjusted using 0.01 M NaOH, after the addition of which, an instant change in color of the reaction mixture was seen. Therefore, the formation of C-AgNPs was monitored primarily by UV–Vis spectroscopy. We varied the amount of NaOH to obtain pH from 5.0 to 11.0. At pH 9.0, a sharp and intense band was seen at 402 nm. When the reaction mixture's pH was lower than 9.0, a continuous decrease in intensity was seen with a red-shift of the peak. Finally, the peak disappeared at pH 5.0. The red-shift of peak shows increased particle size with polydispersity. However, at pH 10 and 11, no notable change was observed in peak position and peak intensity (Fig. 5). The corresponding change in color of C-AgNPs is shown in inset of Fig. 5. Thus, we optimized the pH of the reaction medium at 9.0 for further studies.

Although cinchona bark extract itself works as both a reducing and stabilizing agent at pH 9.0, this phenomenon did not work when the pH of the reaction lowered from 9.0. This may be due to pH-dependent redox nature of active components of bark extract. The strong acidic or alkaline condition reduces the active compounds' capacity, which is completely deactivated, thus slowing down the formation of AgNPs.

In most of the reports, nanoparticles' photosynthetic protocols were not efficient to produce nanoparticles with uniform shape and size (Annadhasan et al., 2015). But, in our study, we successfully synthesized mainly spherical particles with a size range of

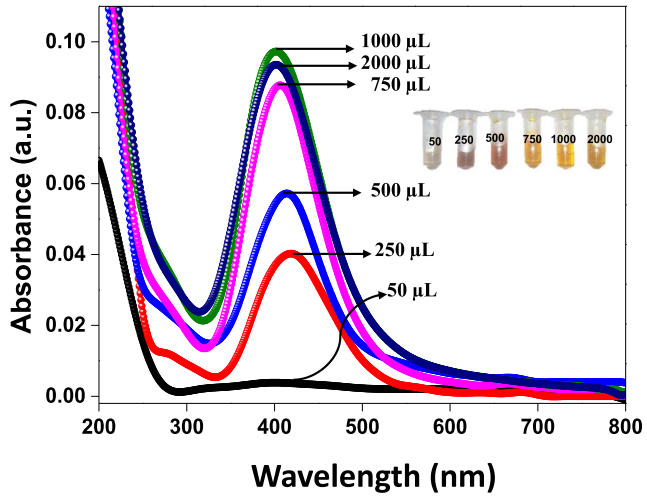

Fig. 4. UV–Vis spectra of AgNPs synthesized by various volumes (50–2000 µL) of cinchona bark extract.

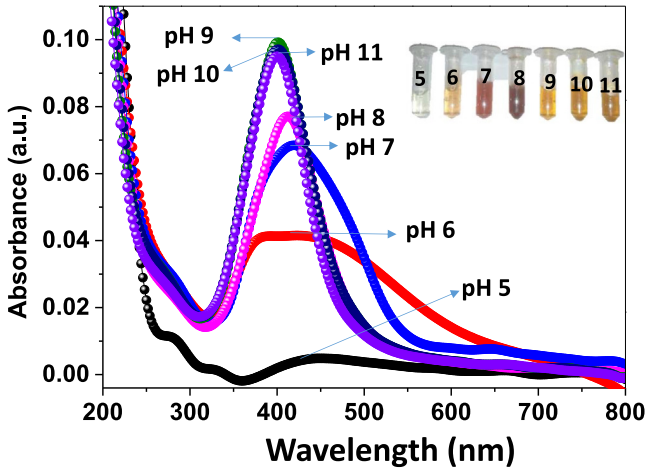

Fig. 5. UV–Vis spectra of C-AgNPs synthesized at different pH ranging from 5 to11.

3–4 nm. Moreover, since we did not use any external stabilizing agent, the synthesis of nanoparticles was not tedious and time-consuming, making the method preferable to other reported methods.

3.3. Selectivity of C-AgNPs

The synthesized C-AgNPs were well dispersed and displayed characteristic yellow color with a strong SPR band at 402 nm. We hypothesized that the C-AgNPs might be developed as an efficient colorimetric sensor to detect toxic metal ions. To demonstrate the sensor's selectivity toward Al^{3+} ion, other environmentally relevant metal ions like Ca^{2+}, Fe^{2+}, Fe^{3+}, Ba^{2+}, Zn^{2+}, Cd^{2+}, Hg^{2+}, Pb^{2+}, Cu^{2+}, Mn^{2+}, Cr^{3+}, and Al^{3+} were also examined under optimized conditions. All the metal ions were added separately into the C-AgNPs solution. On addition of Al^{3+} to the C-AgNPs solution, an instant change in color from dark yellow to brown was observed. This may be due to decreased distance between nanoparticles on the interaction of Al^{3+} with active components in bark extract. However, it was observed that other metal ions induced no or a very slight change in the color of C-AgNPs solution (Fig. 6a). Correspondingly the SPR peak at 402 nm shows a decrease in intensity with a slight red-shift in the presence of Al^{3+}. This red-shift of the peak could be attributed to aggregation of nanoparticles (Saion et al., 2013). UV–Vis spectra of C-AgNPs in the presence of other metal ions were also obtained. The noticeable decrease in intensity with red-shift is a unique feature for the Al^{3+} containing AgNPs (Fig. 6b). The selectivity of C-AgNPs towards various metal ions was further showed by plotting the absorption of the C-AgNPs solution in the presence of each metal ion. The selectivity of C-AgNPs for Al^{3+} was demonstrated by comparing absorption difference (A_0-A) with that of a solution containing other metal ions as shown in Fig. 6c. A higher absorbance difference in absorbance indicates aggregated particles and a lower difference indicates well-dispersed particles (Irfan et al., 2020). A much higher value of A_0-A was seen for C-AgNPs in the presence of Al^{3+} ions compared to that with other metal ions. Hence, AgNPs synthesized by cinchona extract responded selectively for Al^{3+} ion as indicated by a much higher increase in A_0-A due to aggregation of C-AgNPs.

For monitoring interference, a solution of metal ions was prepared by mixing Al^{3+} with other metal ions. Prepared metal ion solution was added to the C-AgNPs solution. Fig. 6d shows that Al^{3+} mixed samples show a change in color of C-AgNPs from dark yellow to brown. These results confirm that other metal ions did not significantly interfere with the detection of Al^{3+} ions. Thus, the colorimetric assay could now be narrowed down to Al^{3+} only, ruling out all another metal ion tested for the selectivity.

3.4. Sensitivity of C-AgNPs

The performance of the developed Al^{3+} sensor is pH-dependent because the pH of the solution influences the synthesis of nanoparticles and affects the interaction between C-AgNPs and Al^{3+} ions. Since the synthesis of C-AgNPs was not much affected by pH in the range of 9.0 to 11.0, we tested the sensor's sensitivity for Al^{3+} in this range. The value of A_0-A was maximum at pH 9.0, as shown in Fig. 7a and in Inset of 7a. This shows that at pH 9.0, bonds between Al^{3+} and cinchona alkaloids formed more easily and resulted in a change in color of the C-AgNPs solution. The color of C-AgNPs changed as the function of Al^{3+} concentration, which was monitored by UV–Vis spectroscopy. The color of the C-AgNPs solution changed progressively from dark yellow to brown and finally started to become transparent, as shown in Fig. 8a. A decrease in intensity at 402 nm with a continuous red-shift was seen with an increasing concentration of 0.01 ppm to 1 ppm (Fig. 8b). The difference in absorption was measured in triplicates for the quantitative detection of Al^{3+}, as shown in Fig. 8c. A linear correlation of the difference in absorption intensity increased linearly with increasing concentration of Al^{3+} in the range of 0.05 ppm to 1 ppm with an R^2 value of 0.9908.

HRTEM and DLS studies were carried to support the results. The aggregation of C-AgNPs in the presence of Al^{3+} was directly supported by HRTEM (Fig. 9a and c) and increased in hydrodynamic diameter from 17 nm to 379 nm as shown by DLS analysis (Fig. 9b and d). This difference in HRTEM and DLS results is because DLS records higher values as light scattered from both core particles and the layer on the surface of nanoparticles, while in the electron-microscopic analysis, only metallic particles core is measured. Zeta potential of the synthesized C-AgNPs was −19.9 mV, which reduced to 13.9 mV on the addition of Al^{3+} (Fig. S3). The change in zeta potential from negative to positive confirms the interaction between negative charges present on the surface of nanoparticles which cause non-cross-linking aggregation of C-AgNPs.

Based on the above results, a possible sensing mechanism of Al^{3+} has been proposed (Scheme 1). Al^{3+} is a hard acid, and it has a strong attraction toward hard bases such as N and O (Chen et al., 2015). Alkaloids present in the bark extract contain N and

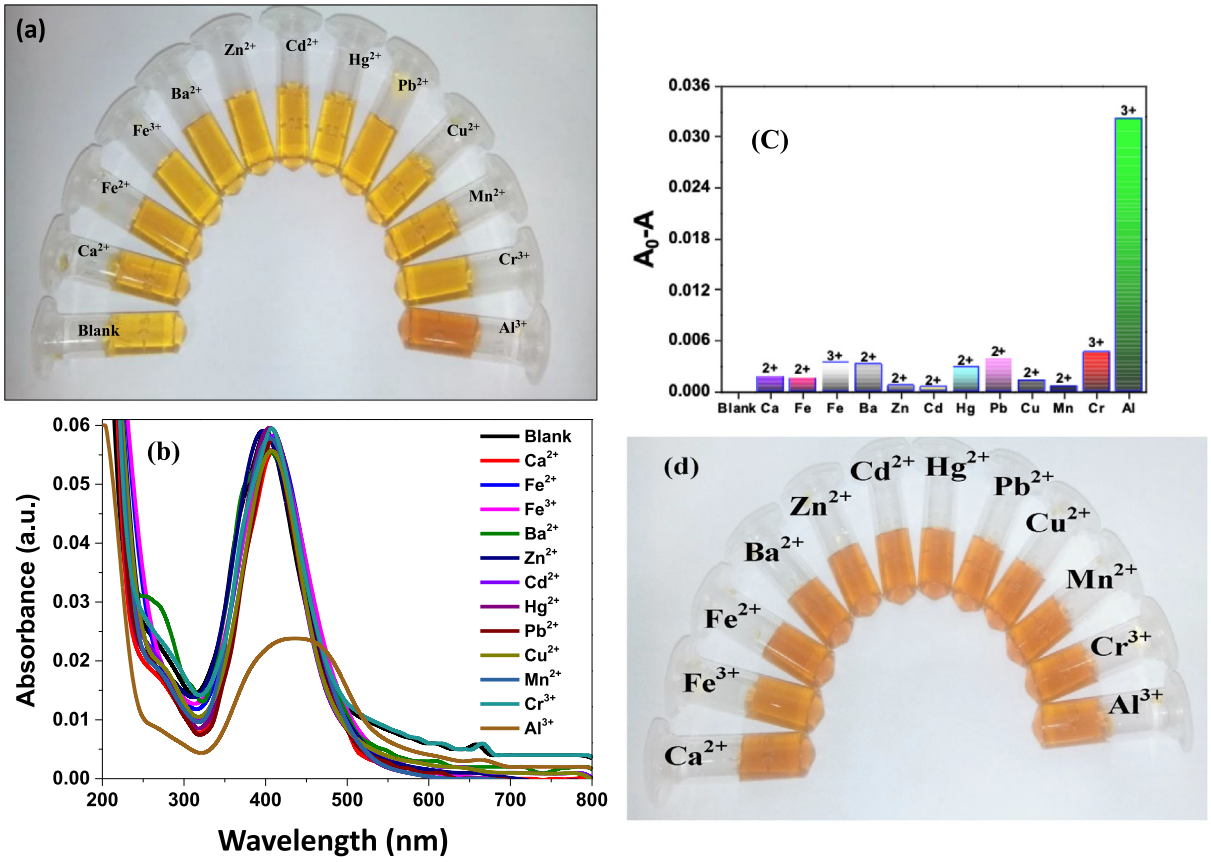

Fig. 6. Photographs show the colorimetric response of C-AgNPs in the presence of various metal ions (a), UV–Vis spectra of C-AgNPs in the presence of different metal ions (b), the corresponding difference in absorbance in the presence of metal ions; each data point is a mean of three measurements; the error bars show standard deviation (c), visual change in color of C-AgNPs in the presence of a mixture of Al^{3+} with other metal ions (d).

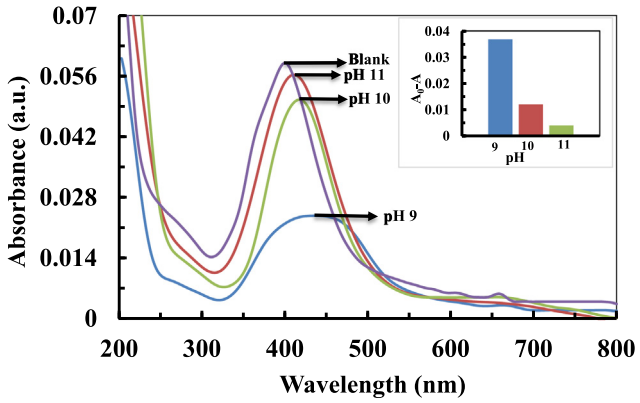

Fig. 7. UV–Vis spectra show the effect of pH on the Al^{3+} sensing; inset bars also represent the effect of pH on sensing of Al^{3+}.

O atoms. Thus, Al^{3+} can coordinate with N and hydroxyl O of alkaloids. This coordination was further confirmed by the FT-IR spectra (Fig. 3c). Two new peaks appeared at 667 cm^{-1} and 1020 cm^{-1}, showing the coordination of N and O to the Al^{3+}. The coordination results in non-crosslinking aggregation of C-AgNPs, which causes a visual change in the color of nanoparticles.

3.5. Application of sensor in a real water sample

To show the applicability of our sensor in real water samples, a recovery test was performed. The concentrations (0.2 ppm and 0.6 ppm) Al^{3+} were spiked in drinking and pond water. These samples were analyzed by using C-AgNPs and AAS. Results from the determination of Al^{3+} ion from water sources are compiled in Table 1. These results show that the proposed method shows good recoveries in the range of 85–108.34%. The results are in accordance with AAS results.

Therefore, this method could be successfully used for the determination of Al^{3+} in real water samples. The performance of the reported colorimetric method was compared with that of several other methods for detecting Al^{3+} (Table S1). Evidently, the present method involves a simple green method for synthesizing AgNPs and allows us to detect Al^{3+} conveniently with a LOD lower than the limit set by USEPA and WHO. Therefore, the present method provides a highly selective and sensitive probe for detecting Al^{3+} ions without any tedious procedure.

4. Conclusion

We successfully fabricated cinchona bark extract stabilized AgNPs by a biocompatible method. The resulting colloidal nanoparticles were used for the detection of Al^{3+} with a LOD of 0.01 ppm. High stability and sensitivity of the probe were obtained at pH 9.0. Change in characteristic SPR band at 402 nm of C-AgNPs in the presence of Al^{3+} ion was due to aggregation of C-AgNPs. The aggregation of nanoparticles was confirmed by HRTEM and DLS analysis. Zeta potential measurement confirms the interaction of Al^{3+} with moiety present on the surface of AgNPs. The synthesized C-AgNPs did not show any interference during detection of Al^{3+} in the presence of other environmentally relevant metal ions. The proposed method was successfully applied to the real water

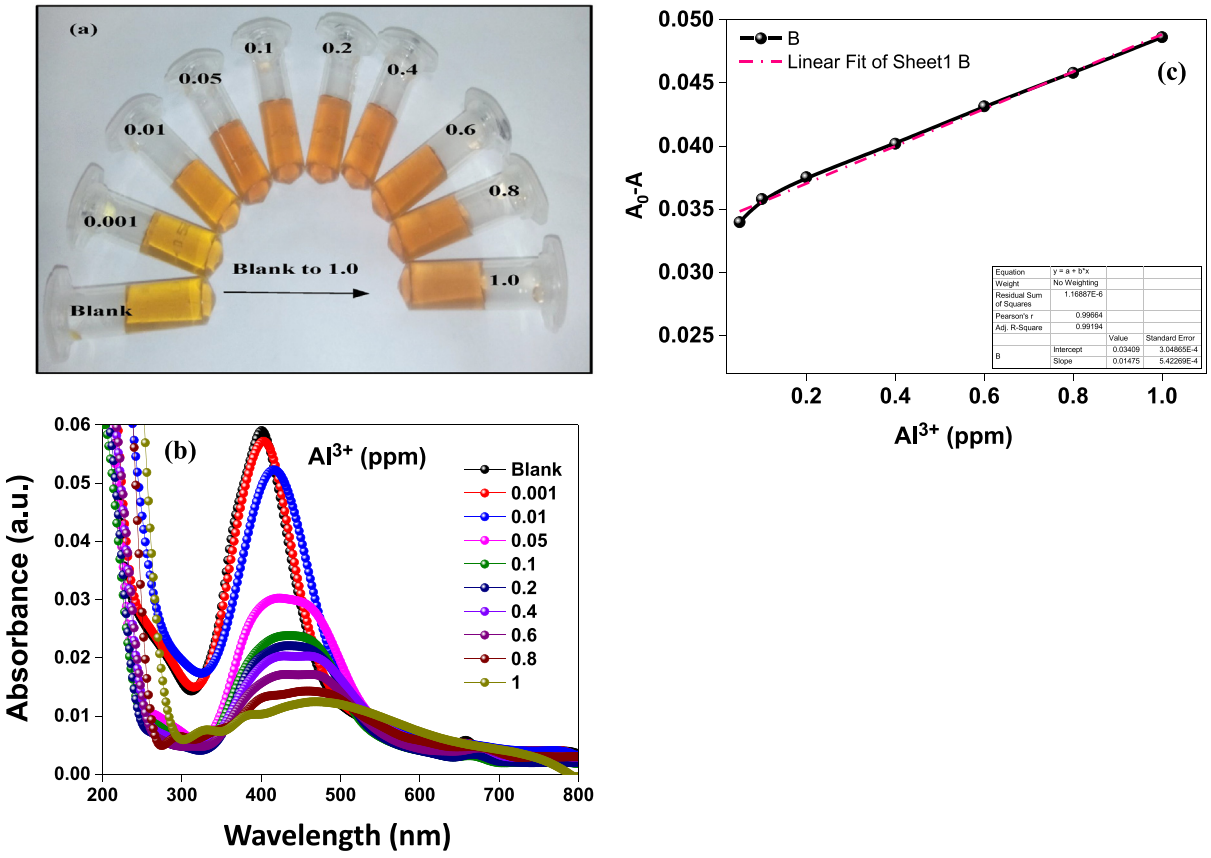

Fig. 8. Optical images showing the visual change in color of C-AgNPs as the function of Al^{3+} concentration (a) UV–Vis spectra of C-AgNPs as the function of the concentration of Al^{3+} (b), calibration plot of the difference in absorbance with various concentration of Al^{3+} showing the linearity of the probe in the range of 0.05–1 ppm (c).

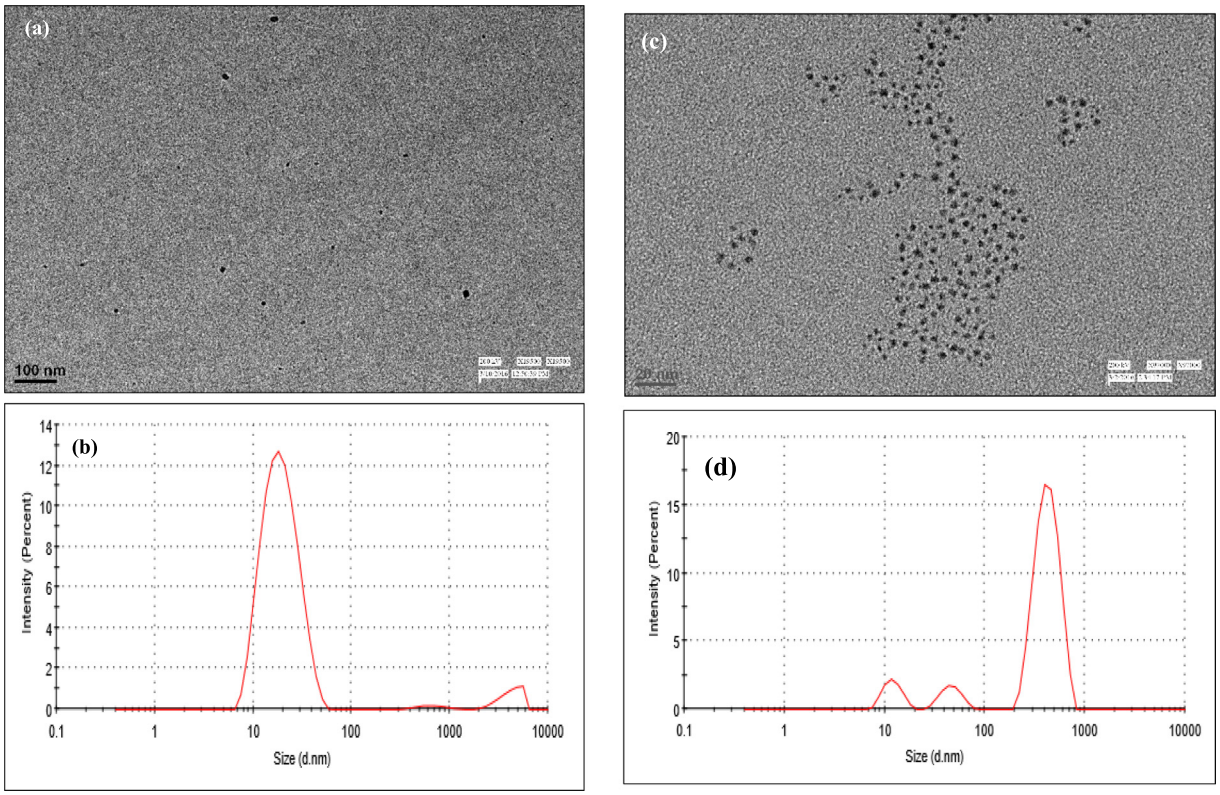

Fig. 9. HRTEM images (a) and size distribution (b) of C-AgNPs in the presence of Al^{3+}, the average diameter of C-AgNPs is 3–4 nm, HRTEM images (c) and size distribution (d) of C-AgNPs in the absence of Al^{3+}.

Table 1
Concentrations of Al^{3+} spiked in drinking and pond water samples measured by C-AgNPs and AAS.

Sample	Added amount (ppm)	Found amount (ppm) (mean ± E, n = 3)	Recovery (%)	AAS
Drinking water	0.2	0.19 ± 0.01	95 ± 5	0.2
	0.6	0.61 ± 0.02	105 ± 3.34	0.59
Pond water	0.2	0.18 ± 0.01	90 ± 5	0.2
	0.6	0.59 ± 0.01	98.33 ± 1.67	0.6

samples analysis. The advantage of the present protocol is a synthesis of mono-dispersed AgNPs with 3–4 nm size by a simple, rapid, cost-effective, and moreover, a biocompatible method that can be used for real water sample analysis.

Declaration of Competing Interest

The authors declare that they have no known competing financial interests or personal relationships that could have appeared to influence the work reported in this paper.

Acknowledgments

Dinesh Kumar is also thankful to DST, New Delhi, for this work's financial support (sanctioned vide project Sanction Order F. No. DST/TM/WTI/WIC/2K17/124(C). The authors extend their sincere appreciation to the Researchers Supporting Project number (RSP-2020/266), King Saud University, Riyadh, Saudi Arabia for the support. Priyanka also thanks AIIMS, New Delhi, and the University of Rajasthan for providing an HRTEM facility.

Appendix A. Supplementary data

Supplementary data to this article can be found online at https://doi.org/10.1016/j.jksus.2021.101527.

References

Abubaker, M., Ngah, C.W.Z.C.W., Ahmad, M., Kuswandi, B., 2018. Colorimetric determination of Al(III) based on the aggregation of gold nanoparticles functionalized with novel 4-benzoyl pyrazolone derivative. AIP Conf. Proc. 1972, 30012. https://doi.org/10.1063/1.5041233.

Achan, J., Talisuna, A.O., Erhart, A., Yeka, A., Tibenderana, J.K., Baliraine, F.N., Rosenthal, P.J., D'Alessandro, U., 2011. Quinine, an old anti-malarial drug in a modern world: role in the treatment of malaria. Malar. J. 10, 144. https://doi.org/10.1186/1475-2875-10-144.

Al-Enizi, A.M., Ubaidullah, M., Ahmed, J., Ahamad, T., Ahmad, T., Shaikh, S.F., Naushad, M., 2020. Synthesis of NiOx@NPC composite for high-performance supercapacitor via waste PET plastic-derived Ni-MOF. Compos. Part B Eng. 183,. https://doi.org/10.1016/j.compositesb.2019.107655 107655.

Al-Hartomy, O.A., Ubaidullah, M., Kumar, D., Madani, J.H., Ahmad, T., 2013. Dielectric properties of Ba1-xSrxZrO3 ($0 \leq x \leq 1$) nanoceramics developed by citrate precursor route. J. Mater. Res. 28, 1070–1077. https://doi.org/10.1557/jmr.2013.40.

Annadhasan, M., Kasthuri, J., Rajendiran, N., 2015. Green synthesis of gold nanoparticles under sunlight irradiation and their colorimetric detection of Ni2+ and Co2+ ions. RSC Adv. 5, 11458–11468. https://doi.org/10.1039/C4RA14034F.

Basiri, S., Mehdinia, A., Jabbari, A., 2018. A sensitive triple colorimetric sensor based on plasmonic response quenching of green synthesized silver nanoparticles for determination of Fe2+, hydrogen peroxide, and glucose. Colloids Surfaces A Physicochem. Eng. Asp. 545, 138–146. https://doi.org/10.1016/j.colsurfa.2018.02.053.

Bhuvaneswari, S., Seetha, M., Chandrasekaran, J., Marnadu, R., Masuda, Y., Aldossary, O.M., Ubaidullah, M., 2021. Fabrication and characterization of p-Si/n-In2O3 and p-Si/n-ITO junction diodes for optoelectronic device applications. Surf. Interf. 23,. https://doi.org/10.1016/j.surfin.2021.100992 100992.

Chen, W., Jia, Y., Feng, Y., Zheng, W., Wang, Z., Jiang, X., 2015. Colorimetric detection of Al(iii) in vermicelli samples based on ionic liquid group coated gold nanoparticles. RSC Adv. 5, 62260–62264. https://doi.org/10.1039/C5RA09099G.

Chen, Y.-C., Lee, I.-L., Sung, Y.-M., Wu, S.-P., 2013. Colorimetric detection of Al3+ ions using triazole–ether functionalized gold nanoparticles. Talanta 117, 70–74. https://doi.org/10.1016/j.talanta.2013.08.054.

Colmenares, J.C., Luque, R., Campelo, J.M., Colmenares, F., Karpiński, Z., Romero, A.A., 2009. Nanostructured photocatalysts and their applications in the photocatalytic transformation of lignocellulosic biomass: an overview. Materials (Basel) 2, 2228–2258. https://doi.org/10.3390/ma2042228.

Dhillon, A., Sapna, Choudhary, B.L., Kumar, D., Prasad, S., 2018. Excellent disinfection and fluoride removal using bifunctional nanocomposite. Chem. Eng. J. 337, 193–200. https://doi.org/10.1016/j.cej.2017.12.030.

Dhillon, A., Sapna, Kumar, D., 2017a. Dual adsorption behaviour of fluoride from drinking water on Ca-Zn(OH)2CO3 adsorbent. Surf. Interfaces 6, 154–161. https://doi.org/10.1016/j.surfin.2017.01.006.

Dhillon, A., Soni, S.K., Kumar, D., 2017b. Enhanced fluoride removal performance by Ce–Zn binary metal oxide: adsorption characteristics and mechanism. J. Fluor. Chem. 199, 67–76. https://doi.org/10.1016/j.jfluchem.2017.05.002.

Faghiri, F., Ghorbani, F., 2019. Colorimetric and naked eye detection of trace Hg2+ ions in the environmental water samples based on plasmonic response of sodium alginate impregnated by silver nanoparticles. J. Hazard. Mater. 374, 329–340. https://doi.org/10.1016/j.jhazmat.2019.04.052.

Firdaus, M., Andriana, S., Elvinawati, Alwi, W., Swistoro, E., Ruyani, A., Sundaryono, A., 2017. Green synthesis of silver nanoparticles using Carica Papaya fruit extract under sunlight irradiation and their colorimetric detection of mercury ions. J. Phys. Conf. Ser. 817, 12029. https://doi.org/10.1088/1742-6596/817/1/012029.

Gao, Y., Feng, B., Miao, L., Chen, Y., Di, J., 2020. Determination of Cr(III) ions based on plasmonic sensing and anodic stripping voltammetry with amplification of Ag nanoparticles. Microchem. J. 157,. https://doi.org/10.1016/j.microc.2020.104995 104995.

Irfan, M., Ahmad, T., Moniruzzaman, M., Bhattacharjee, S., Abdullah, B., 2020. Size and stability modulation of ionic liquid functionalized gold nanoparticles synthesized using Elaeis guineensis (oil palm) kernel extract. Arab. J. Chem. 13, 75–85. https://doi.org/10.1016/j.arabjc.2017.02.001.

Kacprzak, K., 2013. Chemistry and Biology of Cinchona Alkaloids 21.

Joshi, P., Painuli, R., Kumar, D., 2017. Label-Free Colorimetric Nanosensor for the Selective On-Site Detection of Aqueous Al3+. ACS Sustainable Chemistry & Engineering 5, 4552–4562.

Kim, W., Lee, G., Kim, M., Park, Joohyung, Jo, S., Yoon, D.S., Park, Y.H., Hong, J., Park, Jinsung, 2018. Al3+ ion sensing at attomole level via surface-potential mapping of gold nanoparticle complexes. Sens. Actuat. B Chem. 255, 2179–2186. https://doi.org/10.1016/j.snb.2017.09.031.

Li, X., Wang, J., Sun, L., Wang, Z., 2010. Gold nanoparticle-based colorimetric assay for selective detection of aluminium cation on living cellular surfaces. Chem. Commun. 46, 988–990. https://doi.org/10.1039/B920135A.

Modrzejewska-Sikorska, A., Konował, E., 2020. Silver and gold nanoparticles as chemical probes of the presence of heavy metal ions. J. Mol. Liq. 302,. https://doi.org/10.1016/j.molliq.2020.112559 112559.

Naushad, M., 2014. Surfactant assisted nano-composite cation exchanger: Development, characterization and applications for the removal of toxic Pb2+ from aqueous medium. Chem. Eng. J. 235, 100–108. https://doi.org/10.1016/j.cej.2013.09.013.

Nozik, A.J., 2010. Nanoscience and nanostructures for photovoltaics and solar fuels. Nano Lett. 10, 2735–2741. https://doi.org/10.1021/nl102122x.

Olenin, A.Y., 2019. Chemically modified silver and gold nanoparticles in spectrometric analysis. J. Anal. Chem. 74, 355–375. https://doi.org/10.1134/S1061934819040099.

Puente, C., Gómez, I., Kharisov, B., López, I., 2019. Selective colorimetric sensing of Zn(II) ions using green-synthesized silver nanoparticles: Ficus benjamina extract as reducing and stabilizing agent. Mater. Res. Bull. 112, 1–8. https://doi.org/10.1016/j.materresbull.2018.11.045.

Rastogi, L., Dash, K., Ballal, A., 2017. Selective colorimetric/visual detection of Al3+ in ground water using ascorbic acid capped gold nanoparticles. Sens. Actuat. B Chem. 248, 124–132. https://doi.org/10.1016/j.snb.2017.03.138.

Saion, E., Gharibshahi, E., Naghavi, K., 2013. Size-controlled and optical properties of monodispersed silver nanoparticles synthesized by the radiolytic reduction method. Int. J. Mol. Sci. 14, 7880–7896. https://doi.org/10.3390/ijms14047880.

Serrano, E., Rus, G., García-Martínez, J., 2009. Nanotechnology for sustainable energy. Renew. Sustain. Energy Rev. 13, 2373–2384. https://doi.org/10.1016/j.rser.2009.06.003.

Shaw, C.A., Tomljenovic, L., 2013. Aluminum in the central nervous system (CNS): toxicity in humans and animals, vaccine adjuvants, and autoimmunity. Immunol. Res. 56, 304–316. https://doi.org/10.1007/s12026-013-8403-1.

Shinde, S., Kim, D.-Y., Saratale, R.G., Syed, A., Ameen, F., Ghodake, G., 2017. A Spectral Probe for Detection of Aluminum (III) Ions Using Surface Functionalized Gold Nanoparticles. Nanomater. (Basel, Switzerland) 7, 287. 10.3390/nano7100287.

Sorenson, J.R., Campbell, I.R., Tepper, L.B., Lingg, R.D., 1974. Aluminum in the environment and human health. Environ. Health Perspect. 8, 3–95. https://doi.org/10.1289/ehp.7483.

Vergara-Barberán, M., Lerma-García, M.J., Simó-Alfonso, E.F., Herrero-Martínez, J.M., 2017. Polymeric sorbents modified with gold and silver nanoparticles for solid-phase extraction of proteins followed by MALDI-TOF analysis. Microchim. Acta 184, 1683–1690. https://doi.org/10.1007/s00604-017-2168-5.

Vinod Kumar, V., Anbarasan, S., Christena, L.R., SaiSubramanian, N., Philip Anthony, S., 2014. Bio-functionalized silver nanoparticles for selective colorimetric sensing of toxic metal ions and antimicrobial studies. Spectrochim. Acta Part

A Mol. Biomol. Spectrosc. 129, 35–42. https://doi.org/10.1016/j.saa.2014.03.020.
Xue, D., Wang, H., Zhang, Y., 2014. Specific and sensitive colorimetric detection of Al3+ using 5-mercaptomethyltetrazole capped gold nanoparticles in aqueous solution. Talanta 119, 306–311. https://doi.org/10.1016/j.talanta.2013.11.012.
Zafer, M., Keskin, C.S., Özdemir, A., 2020. Highly sensitive determination of Co(II) ions in solutions by using modified silver nanoparticles. Spectrochim. Acta Part A Mol. Biomol. Spectrosc. 239,. https://doi.org/10.1016/j.saa.2020.118487 118487.
0. Dictionary of Alkaloids. Second Edition with CD-ROM. Anticancer Res. 30, 1036.